CHEMICAL AND PROCESS ENGINEERING
28, 307–321 (2007)

MICHAŁ KARCZ

PERFORMANCE OF A TUBULAR FUEL CELL WITH INTERNAL METHANE REFORMING

Institute of Fluid Flow Machinery, Polish Academy Sciences, Gdańsk

The numerical model of a solid oxide fuel cell fuelled with methane internal reforming is presented in the paper. The model has been implemented into the commercial CFD code. The basic model for fuel cell fed with humidified hydrogen has been extended to cope with mixture of hydrogen, carbon monoxide and methane as a fuel. Numerical calculations have been performed to predict the tubular fuel cell performance for various current densities, electrochemical reaction rate ratio and steam-to-carbon ratio.

Przedstawiono model ogniwa paliwowego SOFC z wewnętrznym reformingiem wraz z wynikami przeprowadzonych obliczeń. Model ten stanowi kolejne rozwinięcie modelu opisującego pracę ogniwa zasilanego czystym wodorem. Rozwinięcie umożliwia zastosowanie modelu do numerycznej analizy ogniw zasilanych mieszaniną wodoru, tlenku węgla i metanu. Przedstawiono wpływ gęstości prądu, współczynnika zachodzenia reakcji elektrochemicznych oraz stosunku strumienia molowego pary wodnej do sumy strumieni molowych wszystkich związków zawierających atomy węgla na pracę pojedynczego tlenkowego ogniwa paliwowego o budowie rurkowej.

1. INTRODUCTION

Direct-oxidation fuel cells seem to be the prospect of modern SOFC systems. Such devices offer a number of advantages over conventional fuel cells employing exclusively pure hydrogen. For example, these fuel cells can use direct conversion of different hydrocarbons, as natural gas, biogas, syngas, LPG, gasoline, diesel and kerosene, to electricity and have a relatively high efficiency. But there are still many problems that should be overcome. One of them is an increase of concentration overpotential due to dilution of higher hydrocarbon fuels at high fuel utilization rate when a noticeable amount of steam is being created. Other problem is related to carbon deposition that can lead to dramatic increase of overpotential at the anodic side of the cell. All of these problems can be partially avoided by using Cu or ceria-supported precious metals instead of Ni as anode constituent. Experimental investigations in this subject are under progress [1, 2]. However, modern solid oxide fuel cells are still basing mainly on pure hydrogen, or hydrogen-carbon monoxide mixture obtained from either exter-

nal or/and internal reforming of methane or methanol. The reforming can be conducted in two ways, i.e. via an external process and as an internal reforming at the anode. External reformer needs however sufficient heat supply to drive the reaction [3, 4]. On the other hand, internal reforming of methane has several advantages, such as a possibility of direct cell cooling due to an endothermic reforming reaction or utilization of steam coming from electrochemical reaction in a reforming process. Internal reforming leads also to more even distribution of hydrogen throughout the cell [5]. If reforming is performed at the anode, the process is usually called a direct-internal reforming (DIR). When the reforming takes place in a separate section of a fuel cell, where electrochemical reactions do not occur, the process is called indirect- or integrated-internal reforming (IIR) [3, 4].

There are only few papers that explicitly give an overview of internal reforming processes in solid oxide fuel cells. Among them, the paper of Hirano et al. [6] presents some of test results from the working fuel cell (3 kW Osaka gas module). Hecht et al. [7] present details of reforming kinetics based on the experimental data also provided by the authors. Another useful experimental data for reforming process in solid oxide fuel cells have been published by Meusinger et al. [8] and Peters et al. [9]. More details on the problem of numerical modelling of solid oxide fuel cells with internal reforming of methane can be found in the papers by Aguiar et al. [3, 10], Bessette et al. [11], Yakabe et al. [12, 13], Campanari and Iora [14], Ackmann et al. [15], Haberman and Young [16], Badur and Lemański [17].

In the following paper, a development of the author model presented in [18] is described. The basic electrochemical reactions for a solid oxide fuel cell fuelled by humidified hydrogen have been extended to cope also with methane and carbon monoxide as the fuel mixture constituents. Beside this, modelling of the diffusion has been modified to include the Knudsen and multi-component diffusion instead of the simple gradient Fick hypothesis. The results of basic computations are compared with the data presented by Campanari and Iora [14] for a similar fuel cell geometry. The model has also been used for parametrical analysis to assess the solid fuel cell performance with an internal reforming process.

2. BASIC REACTIONS IN SOFC WITH INTERNAL REFORMING

The electrochemical processes of the solid oxide fuel cell occur in the porous electrodes. Anode electrodes are usually composed of a ceramic–metal composite with yttria-stabilized zirconia (YSZ) as the ceramic component and Ni for the metal component [2, 7]. Such *cermet* shows a good thermal-expansion performance, simultaneously being a good electronic conductor and an excellent steam-reforming catalyst. The electrolyte layers are rather thin, dense YSZ and the cathode electrodes are usually based on strontium-doped lanthanum manganite La/Sr/MnO_3 [23]. In the case of electrode supported fuel cells, the electrolyte should be as thin as possible to lower the

ohmic polarization and to allow the cell to operate at temperature lower than 800 ºC [3, 23, 26]. On the other hand, the electrolyte-supported fuel cells are dedicated for operating at about ~1000 ºC due to rather high electrolyte resistivity at lower temperature [26].

In a tubular SOFC, the oxidant diffuses through the porous support tube that is a base for electrodes and electrolyte. On the cathode, the oxygen molecules are being reduced to ions (Eq. (1)), which migrate throughout the electrolyte to the anode where water and carbon dioxide are created and electrons are released due to oxidation (Eq. (2)). The electrons that are passed back via an external circuit to the cathode allow the next oxygen molecules being reduced. They are responsible for the generation of electrical current which is equal the Faraday number F times the mole stream of hydrogen and carbon monoxide. Elementary electrochemical reactions of solid oxide fuel cells fuelled by humidified hydrogen involve only reduction at the cathode:

$$\frac{1}{2}\mathrm{O_2} + 2\mathrm{e^-} \rightarrow \mathrm{O^{2-}} \tag{1}$$

and oxidation reaction at anode:

$$\mathrm{H_2} + \mathrm{O^{2-}} \rightarrow \mathrm{H_2O} + 2\mathrm{e^-} \tag{2}$$

If we consider a fuel cell fed by methane via steam-reforming reaction, it should be noticed that carbon monoxide, which is one of the products, can be also electrochemically converted at the anode via the following reaction:

$$\mathrm{CO} + \mathrm{O^{2-}} \rightarrow \mathrm{CO_2} + 2\mathrm{e^-} \tag{3}$$

Solid oxide fuel cells are dedicated to employ higher hydrocarbon fuels. Reforming with steam gives the mixture of hydrogen and carbon monoxide. The relevant process is governed by a general reaction [4, 28]:

$$\mathrm{C}_n\mathrm{H}_m + \left(\frac{1}{2}m - 1\right)\mathrm{H_2O} \rightarrow (m-1)\,\mathrm{H_2} + n\mathrm{CO} \tag{4}$$

It should be underlined however, that even for simple hydrocarbons as methane, due to some problems related to complete the reaction, some degree of fuel prereforming should be always considered [29]. It is especially important for higher hydrocarbons due to much lower cracking temperature than that of methane. A part of carbon monoxide that does not react electrochemically is converted into carbon dioxide via shift reaction

$$\mathrm{CO} + \mathrm{H_2O} \rightarrow \mathrm{CO_2} + \mathrm{H_2} \tag{5}$$

This reaction is also a source of additional hydrogen working in the cell. Previous investigations revealed that the gas shift reaction in porous anodes lower the concentration polarization [23], because it prevents the increase of CO concentration at the

anode [27]. Thus steam needs to be added in some excess of the stoichiometric requirement of the reforming reaction (4) that simultaneously leads to an enhancement of shift reaction (5) and results in CO depletion.

3. NUMERICAL MODEL

The same procedure as in author's previous paper is currently employed [18]. Moreover, similar geometrical configuration of a tubular fuel cell is being considered with characteristic dimensions which have been taken from the paper of Campanari and Iora [14]. The geometrical model is presented schematically in Fig. 1. The details of mathematical model employed for humidified hydrogen fuelled SOFC one can find in the previous author's paper [18]. The model has been verified and the performance of a tubular fuel cell under various operation regimes has been investigated.

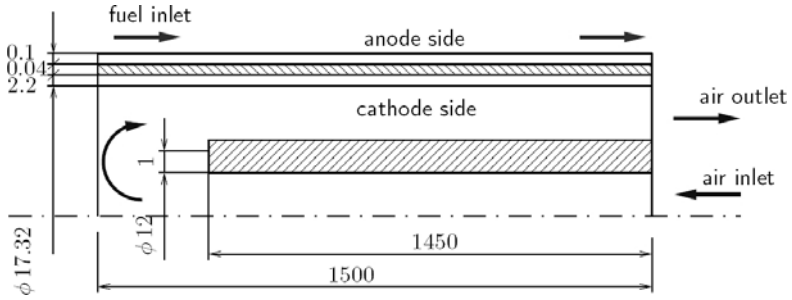

Fig. 1. Geometry of a tubular fuel cell with characteristic dimensions as in [14]

However, there are some differences between previous and present model that should be pointed. As long as the reactions occurring during fuel cell operation have a different thermal impact on the system, it should be included in the overall energy balance. Reaction of water creation (2) is strongly exothermic (ΔH = –241 kJ/mol [22]). The same is for oxidation of carbon monoxide (3) (ΔH = –283 kJ/mol [22]). Apparently the steam-reforming reaction (4) is strongly endothermic (ΔH = 206 kJ/mol [22]). It can lead to dangerous local subcooling and high thermal stresses in the fuel entrance section [20]. On the other hand, water-gas shift reaction (5) is slightly exothermic (ΔH = –41 kJ/mol [22]).

An external pre-reformer where part of methane is being reformed is needed due to some limitations of the internal reforming process. As a result, at the fuel cell inlet a mixture of CH_4, CO, CO_2, H_2O and H_2 is present. It is quite different from the original model where only H_2 and H_2O have been used at the anodic side. The model has been extended then to cope with new species by means of additional transport equations and multi-component diffusion.

Important changes have also been introduced to the relation which governs the fuel mass flow rate m_f to meet the required value of the average current density i_{avg} based on the fuel utilization factor U_f:

$$m_f = \frac{i_{\text{avg}} A_{\text{cell}}}{2FU_f} \cdot \frac{\bar{M}}{\left(X_{\text{H}_2} + X_{\text{CO}} + 4X_{\text{CH}_4}\right)} \tag{6}$$

On the other hand, the definition of air mass flow rate throughout the cell has not been changed. Voltage generated in the fuel cell is calculated via the Nernst equation which has been extended to include CO electrochemistry:

$$\begin{aligned} \Delta E = \beta & \left[\frac{-\Delta G^{\circ}_{\text{H}_2\text{O}}}{2F} + \frac{RT}{2F} \ln\left(\frac{X_{\text{H}_2} X^{0.5}_{\text{O}_2}}{X_{\text{H}_2\text{O}}} \right) \right] \\ & + (1-\beta) \left[\frac{-\Delta G^{\circ}_{\text{CO}_2}}{2F} + \frac{RT}{2F} \ln\left(\frac{X_{\text{CO}} X^{0.5}_{\text{O}_2}}{X_{\text{CO}_2}} \right) \right] + \frac{RT}{4F} \ln\left(p_0 \right) \end{aligned} \tag{7}$$

The coefficient β is a split factor that will be discussed later. Equation (7) gives the theoretical value that should be lowered by several losses at both anode and cathode sides:

$$V = \Delta E - \eta_{\text{act}} - \eta_{\text{conc}} - \eta_{\text{ohm}} \tag{8}$$

Activation polarizations are important for lower values of the current density. Concentration polarization became dominant at higher current densities and some limiting current density is always noticed when the mole fraction of diluent gas is more than 40% [23]. The closure for relevant voltage losses i.e. η_{act} activation, η_{conc} concentration and η_{ohm} ohmic polarizations are also described in [18]. However, in the present analysis the values of exchange i_0 and limiting i_L current densities at the both cell sides have been calculated based on the equation given by Campanari and Iora [14] and Jiang and Virkar [23], rather than being explicitly assumed. Ohmic polarisation η_{ohm} includes also losses generated in the fuel cell interconnector. The characteristic thickness and specific resistivity of the interconnector are taken from [14].

3.1. ELECTROCHEMICAL REACTIONS

There are some ambiguities on the ratio of H_2 and CO consumption due to electrochemical reactions (2) and (3). In the paper by Bessette et al. [11], it was analytically assumed as equal 3:1, while Yakabe et al. [12, 13] have employed the ratio 2:1 obtained experimentally. Matsuzaki and Yasuda [27] found experimentally that the ratio of the electrochemical oxidation rate of CO to H_2 is higher than 1.9 at 1023 K and 2.3 at 1273 K. Some authors, however, assume that the electrochemical conversion rate of CO may be totally neglected [16].

In the present modelling, the effect of various reaction rates of electrochemical oxidation of H_2 and CO is included via the split β factor:

$$\beta = \frac{rX_{H_2}}{rX_{H_2} + X_{CO}} \tag{9}$$

where r is the electrochemical reactions rate ratio.

3.2. REFORMING AND WATER-GAS SHIFT REACTION

Steam-reforming reaction (4) is very fast at high temperatures. For example, at 900 ºC its rate is over 40 times higher than the electrochemical reaction rate [22], and at 1000 ºC this ratio reaches 80 [20]. The water-gas shift reaction is also fast enough to be treated as being in chemical equilibrium in the anode [12]. In the paper by Hecht et al. [7], one can find information on full mechanism of reforming- and water-gas shift reactions within Ni-YSZ anode, including also surface chemistry. The model involves 42 steps and is currently tested. It is, however, time-consuming and its implementation is rather difficult. The reaction rate of methane reforming on Ni-YSZ electrode is then usually given as a function of methane and steam concentrations. Following the paper by Ahmed and Foger [5], a general equation can be written in the form:

$$r^R = k p_{CH_4}^{\alpha} \, p_{H_2O}^{\beta} \tag{10}$$

Similar equations have been adopted by Campanari and Iora [14], and also by Yakabe et al. [12]. Some authors argue that the reforming process is linearly dependent on methane concentration only. Then the reaction rate can be formulated as a first-order kinetics ($\alpha = 1$) with respect to methane and zero-order to steam ($\beta = 0$) [24] but generally Eq. (10) is valid for $\alpha = (0.85–1.3)$ and $\beta = –(1.28–0.35)$ [12, 5, 14, 20]. The reaction rate constant k in Eq. (10) is defined the Arrhenius equation. There are many discrepancies, however in the k values reported in the literature due to various anodes composition [5].

Equations enabling estimation of forward and backward rates of species creation/destruction for reforming (4) and water-gas shift (5) reactions are given by Lehnert et al. [22]:

$$r^R = k_r^+ p_{CH_4} p_{H_2O} - k_r^- p_{CO} p_{H_2}^3 \tag{11}$$

$$r^S = k_s^+ p_{CO} p_{H_2O} - k_r^- p_{CO_2} p_{H_2} \tag{12}$$

where k_r and k_s denote the rate constants of reforming and shift reaction for forward (+) and backward (–) directions, respectively. The rate constants are temperature dependent and these can be found in the original paper [22]. Such assumption is also

employed in the papers by Yuan and Sunden [31], Haberman and Young [16, 30], as well as in the present study.

3.3. THERMODYNAMIC AND TRANSPORT PROPERTIES OF SPECIES

Analysis of thermodynamic and transport phenomena has been presented by Achenbach [20], Haberman and Young [30], Lehnert et al. [22], Yuan and Sunden [31]. The diffusion process is very important in solid oxide fuel cells due to porosity of electrodes which cause that the momentum of fuel gas is nearly zero at the cathode and anode. The rate of diffusion of a reactant influences electrochemical reactions for high current density and fuel utilization rate [13]. In the previous author's analysis of a fuel cell performance, a simple gradient Fick hypothesis has been employed [18]. The Fickian diffusion assumption is valid rather for dilute and binary mixtures. However in multi-component systems as in the case of a fuel cell with internal methane reforming a multi-component diffusion model should be used. In the present analysis, a variant of the mean transport pore model (MTPM) has been employed [13, 15, 22].

The effective value of the diffusion coefficient for k component of the mixture takes into account molecular $D_{k,m}$ and Knudsen $D_{k,K}$ diffusion. The diffusion is also dependent of porosity to tortuosity ratio τ that accounts for the complex structure of electrodes, where the diffusion path length along the pores is greater than a normal electrode thickness [3]:

$$D_k^{\text{eff}} = \frac{\varepsilon}{\tau}\left(D_{k_m} + D_{kK}\right) \tag{13}$$

Knudsen diffusion of k-component of the mixture is defined as [22, 13]:

$$D_{kK} = \frac{2}{3}\left(\frac{8RT}{\pi M_k}\right)^{1/2} \bar{r} \tag{14}$$

where $\bar{r}$ represents the average radius of the pore. Molecular diffusion $D_{k,m}$ is a function of the binary diffusion coefficient D_{kl} of species k and any other constituent l present in the mixture:

$$D_{km} = \frac{1 - Y_k}{\sum_{k \neq l} \frac{Y_l}{D_{kl}}} \tag{15}$$

The binary diffusion coefficients can be either derived based on the Chapman –Enskog theory as in [13] or can be directly taken from [31].

3.4. MATERIAL PROPERTIES OF FUEL CELL CONSTITUENTS

The analysis of various thermodynamic and material properties necessary to perform SOFC computations one can find in the paper by Kowalczyk et al. [21]. The porosity ε, tortuosity τ and the mean pore size $\bar{r}$ that govern the diffusion process are the main parameters of the electrodes. The anode porosity measured by Kim et al. was equal 38% and the cathode porosity was about 30% [25]. In other experimental study, Matsuzaki and Yasuda employed anode with 45% porosity [27]. For example Yakabe et al. [13] have employed the porosity value $\varepsilon = 46\%$, tortuosity factor $\tau = 4.5$, and the average pore size 2.6 μm. Generally porosities of electrodes range from 20 to 60, and tortuosity factors τ vary between 2 and 10 for various porous bodies, and the typical mean pore size lies in the range of 0.5–10 μm [25, 15, 3, 16, 7, 30]. In the present analysis, the porosity value $\varepsilon = 50\%$, tortuosity factor $\tau = 3$ and pore radius $\bar{r} = 1$ μm for both cathode and anode electrodes have been assumed.

4. COMPUTATIONS

In the first step, the implemented model has been compared with the data of Campanari and Iora [14] for similar geometry and boundary conditions. Next, the influence of electrochemical reaction rate ratio r has been investigated. At the end, the fuel cell performance has been computed for various steam-to-carbon ratios S/C. Similarly as in the papers of Yakabe et al. [13], Aguiar et al. [10], Haberman and Young [16], and Campanari and Iora [14], the uniform average current density i_{avg} throughout the cell have been employed. The boundary conditions for fuel and oxidizer compositions and flow rates have been collected from the papers by Campanari [28], Campanari and Iora [14], Haberman and Young [16], Hirano et al. [6].

4.1. NUMERICAL PROCEDURE

For the numerical modelling, the commercial code Fluent [32] has been employed. The model has been implemented into the solver by means of external user-defined subroutines (UDF). Such a numerical technique allows one to solve the problem of electrochemical reactions in SOFC [32]. Similarly as in [18], ideal gas mixture, incompressible and laminar flow and homogenous and isotropic nature of electrodes have been assumed. No radiative heat transfer has been considered in this study. Only a single tubular fuel cell has been investigated, as in Fig. 1. The geometrical model has been prepared as 2D axisymmetric case. The density of the numerical grid for geometry discretization was determined on the basis of the sensitivity studies.

4.2. DISCUSSION OF THE RESULTS

The distributions of the species mole fractions at the anode side of the fuel cell for the assumed average current density $i_{avg} = 1800$ A/m^2, fuel utilization factor $U_f = 0.69$

and air utilization factor $U_a = 0.178$, are presented in Fig. 2. At the cell entrance region, there is a drop of mole fractions of methane, carbon dioxide and steam due to the reforming reaction (4), and water-gas shift reaction (5) that initially runs in backward direction. Due to a high rate of the reforming process, methane has already been consumed at the inlet region that extends to about 30% of the length of the cell. Similar results are reported by Aguiar et al. [3, 10] Campanari and Iora [14] and also by Hirano et al. [6] for low current densities $I < 2000$ A/m^2. When methane is being totally depleted, there is a slight change in distribution of other species due to the termination of the reforming reaction (5). The formation of CO_2 and H_2O is then growing, because the fuel cell electrochemical oxidization reactions (2) and (3) become dominant [14].

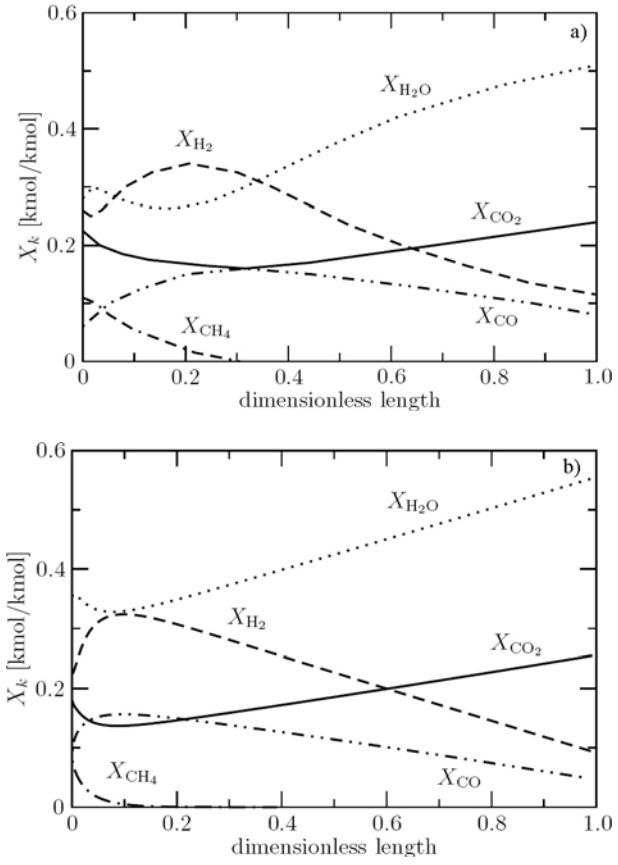

Fig. 2. Distribution of species at the anode:
a) data taken from [14], b) present calculations

The distributions of particular species along the cell length(Fig. 2) are similar to those presented in the paper by Aguiar et al. [3] and also by Campanari and Iora [14]. The differences in the length of methane depletion result from assumed kinetics of the

reforming process. Previous investigations employ rather a simple formulation as (10) In the present study more detailed model with the reaction rate based on Eqs. (11) and (12) has been used. In general, the results obtained are in agreement with the data from [14], despite of the model differences. The same level of generated voltage, i.e. (0.72 V and 0.69 V, respectively) and power (101 W and 103.8 W) has been noticed for the same boundary conditions and identical current density $i = 1800$ A/m^2.

The reforming process affects strongly the temperature distribution in the cell. For the humidified hydrogen fuelled SOFC, the overall mean temperature rises with the current density. In the case of fuel cell with an internal reforming as in the present case temperature is almost equal for various current densities. This is not valid however for low current densities 50–1000 A/m^2 where temperature rises dramatically. There can also be observed some temperature drop for extremely low current densities ($I < 50$ A/m^2). It is shown in Fig. 3.

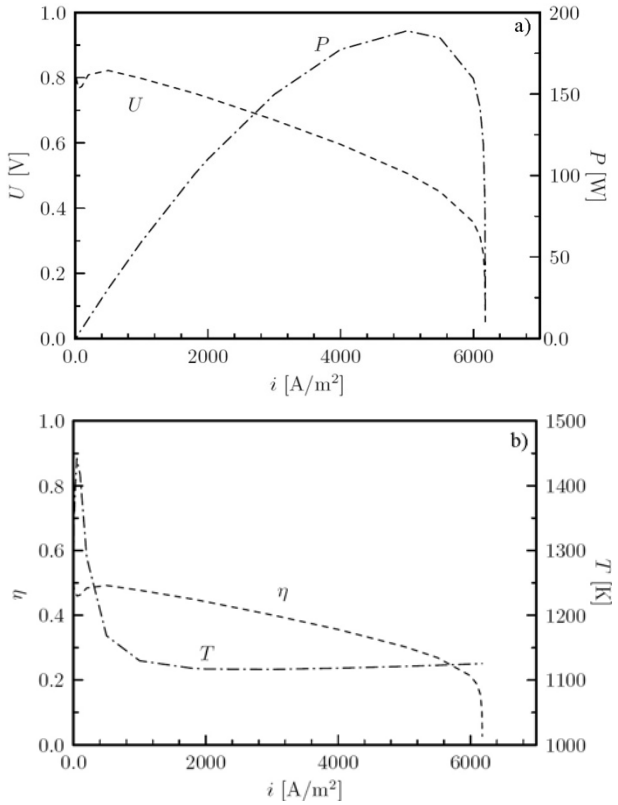

Fig. 3. Changes of characteristic fuel cell parameters as a function of current density: a) voltage and power, b) temperature and efficiency

These temperature changes influence also the voltage generation in the fuel cell. For humidified hydrogen fuel cell, voltage grows continuously with lowering current

density. In the present case, on the other hand, there is a drop of voltage for a low range of current densities. It is a result of strong dependence of the standard Nernst potential (7) on temperature. The changes of power and efficiency are also shown in Fig. 3. The shape of the power curve is however similar to those obtained with humidified hydrogen fuel [18]. The maximum of the efficiency curve, that strongly correlates with the voltage highest value, reaches 50%. The influence of electrochemical reaction rate ratio r on the results is also important as can be seen in Fig. 4.

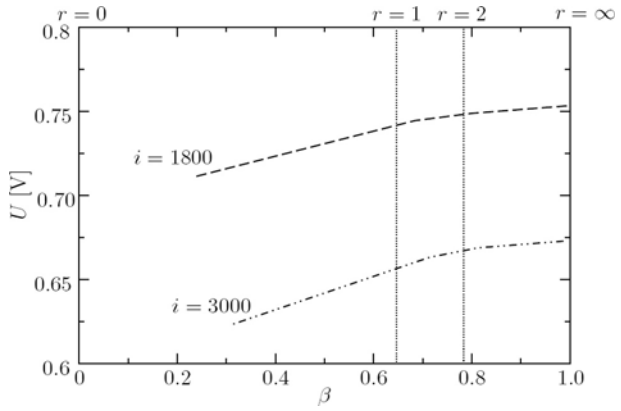

Fig. 4. Voltage generation for different electrochemical reaction rate ratio r

Modelling of voltage generation in a fuel cell depends on the assumption whether it is pure H_2 ($r = \infty$) or pure CO ($r = 0$) electrochemistry. The voltage difference reaches about 0.03–0.05 V, efficiency 3–5% and power 5–12 W for the mean current density equal 1800–3000 A/m^2, respectively. During further computations, the electrochemical reaction rate ratio $r = 2$ has been assumed for determination of the split factor β via Eq. (9), which is consistent with the data from Yakabe et al. [12, 13] and Matsuzaki and Yasuda [27].

The steam-to-carbon ratio S/C is the ratio of the number of steam molecules to the number of carbon atoms inside the cell. Internal steam reforming has a limitation due to carbon deposition and cell deactivation for S/C $<$ 3 [19]. It is strongly coupled with the increase of carbon monoxide content due to reaction (4), for lower S/C, and limiting capabilities of CO consumption via water-gas shift reaction (5). So sufficient amount of steam should be provided to assure a proper cell performance, either from external sources or as internal product of the electrochemical reaction (2). Generally for standard Ni-YSZ electrode S/C should even range from 3 to 5 to fully avoid carbon formation at the anode [5]. Some results available in the literature point however that for particular cases the steam-to-carbon ratio can be lowered even to 1 but only in the case of relatively low methane fraction [6] or when modified Ni-based anodes are employed [5].

The influence of steam-to-carbon ratio on fuel cell performance is presented in Fig. 5. Various S/C values have been obtained through addition of steam at the cell

inlet. Mole streams of the rest of species in the fuel mixture became unchanged and the air mass flow rate has been governed via constant air utilization factor $U_a = 0.178$. When the steam-to-carbon ratio becomes higher, the overall current density and fuel cell power also grow. Simultaneously, a noticeable voltage and efficiency drop can be observed.

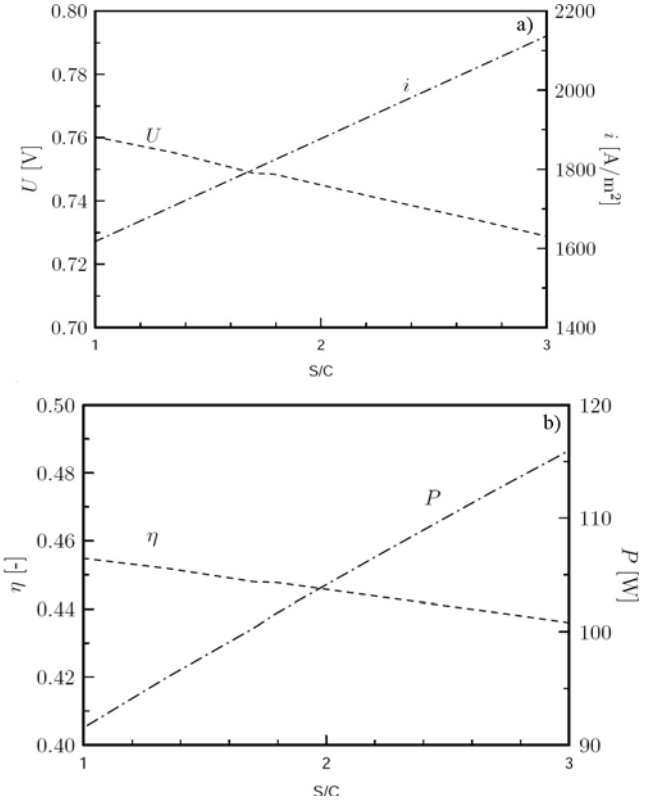

Fig. 5. Dependence of general fuel cell performance on the steam-to-carbon ratio S/C at the cell inlet: a) current density and voltage, b) power and efficiency

5. CONCLUSIONS

The results of numerical computations for tubular solid oxide fuel cell with internal methane reforming are presented. The model employed in the study was built on the assumption of constant average current density thorough the cell. Voltage has been estimated from the Nernst equation and polarizations which were influenced by temperature.

The reforming and water-gas shift processes have been modelled with the kinetics provided by Lehnert at al. [22]. The material properties were assumed based on the data collected from operating fuel cells. The results are in an agreement with the numerical and experimental data presented elsewhere. The model implemented gives an

opportunity of performing a full analysis of fuel cells of various types in terms of geometry, materials and parameters.

Present numerical analysis have revealed that there are a lot of parameters that should be investigated and included during computations of solid oxide fuel cell with direct methane reforming. For example, the influence of electrochemical reaction rate ratio r on the results is noticeable, and cannot be simply neglected. As far as almost all fuel cell characteristic parameters are governed by temperature, there is a strong dependence of temperature on the fuel cell performance. Further investigations are under progress.

ACKNOWLEDGEMENTS

The author would like to express his gratitude to Prof. J. Badur, Mr. M. Lemański and Mr. S. Kowalczyk for valuable discussions and their support on this work. This research has been supported by the State Committee of Scientific Research (KBN) under the contract No. 3T10B 05026.

SYMBOLS

A – area, m^2
D – diffusivity coefficient, m^2/s
F – Faraday constant, C/mol
i – current density, A/m^2
k – reaction rate constant
m – mass flow rate, kg/s
M – molecular weight, kg/kmol
$\bar{M}$ – mean molecular weight, kg/kmol
p – pressure, Pa
r – electrochemical reaction rate ratio
R – gas constant, J/(mol·K)
T – temperature, K
U – utilization factor (fuel, oxidizer)
X – mole fraction
Y – weight fraction
β – split factor
ε – porosity factor
η – voltage losses, V
λ – heat conductivity coefficient, W/(m·K)
τ – tortuosity factor

SUBSCRIPTS AND SUPERSCRIPTS

+ – forward
– – backward
0 – standard, referential
a – air
act – activation
avg – average
conc – concentration
eff – effective
f – fuel

385 k, l – components of mixture
386 ohm – ohmic
387 r, R – reforming
388 s, S – water-gas shift reaction
389 α, β – reaction rate exponents

390 REFERENCES

391 [1] SASAKI K., WATANABE K., SHIOSAKI K., SUSUKI K., TERAOKA Y., J. Electroceram., 2004, 13, 669.
392 [2] KIM H., PARK S., VOHS J.M., GORTE R.J., J. Electrochem. Soc., 2001, 148, A693.
393 [3] AGUIAR P., ADJIMAN C.S., BRANDON N.P., J. Power Sources, 2004, 138, 120.
394 [4] CLARKE S.H., DICKS A.L., POINTON K., SMITH T.A., SWANN A., Catal. Today, 1997,38, 411.
395 [5] AHMED K., FÖGER K., Catal. Today, 2000, 63, 479.
396 [6] HIRANO A., SUZUKI M., IPPOMMATSU M., J. Electrochem. Soc., 1993, 2744.
397 [7] HECHT E.S., GUPTA G.K., ZHU H., DEAN A.M., KEE R.J., MAIER L., DEUTSCHMANN O., Appl. Catal.
398 A: General, 2005, 295, 40.
399 [8] MEUSINGER J., RIENSCHE E., STIMMING U., J. Power Sources, 1998, 71, 315.
400 [9] PETERS R., DAHL R., KLÜTTGEN U., PALM C., STOLTEN D., J. Power Sources, 2002, 106, 238.
401 [10] AGUIAR P., CHADWICK D., KERSHENBAUM L., Chem. Eng. Sci., 2002, 57, 1665.
402 [11] BESSETTE II N.F., WEPFER W.J., WINNICK J., J. Electrochem. Soc., 1995, 11, 3792.
403 [12] YAKABE H., OGIWARA T., HISHINUMA M., YASUDA I., J. Power Sources, 2001, 102, 144.
404 [13] YAKABE H., HISHINUMA M., URATANI M., MATSUZAKI Y., YASUDA I., J. Power Sources, 2000, 86, 423.
405 [14] CAMPANARI S., IORA P., J. Power Sources, 2004, 132, 113.
406 [15] ACKMANN T., DE HAART L.G.J., LEHNERT W., STOLTEN D., J. Electrochem. Soc., 2000, 150, A783.
407 [16] HABERMAN B.A., YOUNG J.B., Int. J. Heat Mass Transfer, 2004, 47, 3617.
408 [17] BADUR J., LEMAŃSKI M., Inż. Chem. Proc., 2005, 26, 157.
409 [18] KARCZ M., Inż. Chem. Proc., 2006, 27, 201.
410 [19] PARK S., CRACIUN R., VOHS J.M., GORTE R.J., J. Electrochem. Soc., 2003, 146, 3603.
411 [20] ACHENBACH E., RIENSCHE E., J. Power Sources, 1994, 52, 283.
412 [21] KOWALCZYK S., KARCZ M., BADUR J., Arch. Therm., 2006, 27, 21.
413 [22] LEHNERT W., MEUSINGER J., THOM F., J. Power Sources, 2000, 87, 57.
414 [23] JIANG Y., VIRKAR A.V., J. Electrochem. Soc., 2003, 150, A942.
415 [24] BELYAEV V.D., POLITOVA T.I., MARINA O.A., SOBYANIN V.A., Appl. Catal. A: General, 1995, 133, 47.
416 [25] KIM J.-W., VIRKAR A.V., FUNG K.-Z., MEHTA K., SINGHAL S.C., J. Electrochem. Soc., 1999, 146, 69.
417 [26] VIRKAR A.V., J. CHEN, C.W. TANNER, J.-W. KIM, Solid State Ion., 2000, 131, 189.
418 [27] MATSUZAKI Y., YASUDA I., J. Electrochem. Soc., 2000, 147, 1630.
419 [28] CAMPANARI S., J. Power Sources, 2001, 92, 26.
420 [29] PETERS R., RIENSCHE E., CREMER P., J. Power Sources, 2002, 86, 432.
421 [30] HABERMAN B.A., YOUNG J.B., ASME J. Fuel Cell Sci. Tech., 2006, 3, 312.
422 [31] YUAN J., SUNDEN B., ASME J. Fuel Cell Sci. Tech., 2006, 3, 89.
423 [32] Fluent Inc., 2005.

424 MICHAŁ KARCZ

425 ANALIZA PRACY RURKOWEGO OGNIWA PALIWOWEGO Z WEWNĘTRZNYM REFORMINGIEM

426 Przedstawiono numeryczny model stałotlenkowego ogniwa paliwowego z wewnętrznym reformin-
427 giem metanu, stanowiący rozwinięcie modelu opracowanego dla ogniw zasilanych czystym wodorem.

Wykorzystano istniejące domknięcia na straty napięcia, wprowadzając wyznaczanie prądu wymiany i_0 i prądu granicznego i_L do szacowania polaryzacji aktywacyjnej i stężeniowej. Doamodelowania procesu reformingu i gazu wodnego zaimplementowano współczynniki postępu reakcji chemicznej przedstawione przez Lehnerta i in. [22]. Wprowadzenie nowych składników reakcji chemicznych i elektrochemicznych, takich jak H_2, H_2O, CO, CO_2, CH_4 wymusiło zmianę sposobu określania współczynników dyfuzji produktów i substratów z równania Ficka. Zastosowano model wieloskładnikowy, uwzględniający także dyfuzję Knudsena w obszarze porowatym. Do określenia napięcia generowanego w ogniwie uwzględniono elektrochemiczną reakcję utleniania H_2 oraz CO przez wprowadzenie współczynnika przebiegu reakcji elektrochemicznych r. Wyniki obliczeń porównano z modelem Campanari i Iora [14] dla takich samych warunków brzegowych i geometrii rurkowego ogniwa paliwowego. Uzyskano podobny rozkład udziałów molowych poszczególnych składników na anodzie, a także zbliżone wartości mocy oraz napięcia. Wykonano charakterystyki pracy ogniwa dla różnych wartości gęstości prądu. W zakresie małych gęstości prądu ($i < 1000$ A/m^2) uzyskano spadek napięcia generowanego w ogniwie z jednoczesnym znacznym wzrostem temperatury. Jest to wynik całkowicie odmienny od rezultatów uzyskanych dla ogniwa zasilanego czystym wodorem. Sprawdzono pracę modelu, założywszy różne wartości współczynnika r. Analiza wykazała, iż uwzględnianie reakcji elektrochemicznego utleniania CO jest istotne ze względu na znaczne różnice generowanego napięcia, mocy i sprawności dla $r = 0$ (tylko reakcja utleniania CO) oraz $r = \infty$ (tylko reakcja utleniania H_2).

Porównano także wpływ liczby S/C, czyli stosunku strumienia molowego pary wodnej do sumy strumieni molowych wszystkich związków zawierających atomy węgla na osiągi rurkowego ogniwa paliwowego. Wzrost S/C przyczynia się do spadków napięcia i sprawności, powodując jednoczesny wzrost gęstości prądu i mocy generowanej w ogniwie.

Received 12 March 2007